HHS Public Access

Author manuscript

Int J Pharm. Author manuscript; available in PMC 2018 June 30.

Published in final edited form as:

Int J Pharm. 2017 June 30; 526(1-2): 69–76. doi:10.1016/j.ijpharm.2017.04.053.

In vivo distribution of zoledronic acid in a bisphosphonate-metal complex-based nanoparticle formulation synthesized by a reverse microemulsion method

Xu Li[1], **Youssef W. Naguib**[1,†], and **Zhengrong Cui**[1,2,*]

[1]The University of Texas at Austin, College of Pharmacy, Division of Molecular Pharmaceutics and Drug Delivery, Austin, Texas

[2]Inner Mongolia Medical University, Inner Mongolia Key Laboratory of Molecular Biology, Hohhot, Inner Mongolia, China

Abstract

Bisphosphonates are used to treat bone diseases such as osteoporosis and cancer-induced bone pain and fractures. It is thought that modifying the pharmacokinetics and biodistribution profiles of bisphosphonates (i.e. rapid renal clearance and extensive bone absorption) will not only reduce their side effects, but also expand their clinical applications to extraskeletal tissues. In the present work, using zoledronic acid (Zol) and calcium as model bisphosphonate and metal molecules, respectively, we prepared DOPA (an anionic lipid)-coated spherical Zol-Ca nanocomposites (Zol-Ca@DOPA) and developed Zol-nanoparticle formulations (i.e. Zol-Ca@bi-lipid NPs) based on the nanocomposites. The influence of the inputted weight ratio of Zol-Ca@DOPA to DSPE-PEG_{2k} on the properties (e.g. size, size distribution, loading efficiency, encapsulation efficiency, zeta potential, and polydispersity) of Zol-Ca@bi-lipid NPs was investigated, and a type of Zol-Ca@bi-lipid NPs with size around 25 nm was selected for further studies. In a mouse model, the Zol-Ca@bi-lipid NPs significantly reduced the bone distribution of Zol, increased the blood circulating time of Zol, and altered the distribution of Zol in major organs, as compared to free Zol. It is expected that similar nanoparticles prepared with bisphosphonate-metal complexes can be explored to expand the applications to bisphosphonates in extraskeletal tissues.

Graphical abstract

*Author of correspondence, Tel: (512) 495-4758, Zhengrong.cui@austin.utexas.edu.

†Current address: Department of Pharmaceutics, Faculty of Pharmacy, Minia University, Minia, Egypt 61111

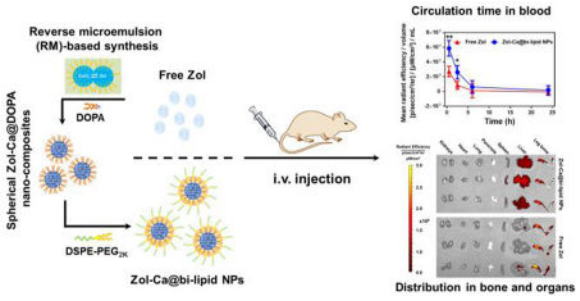

Keywords

zoledronic acid-calcium complexes; in vitro release; pharmacokinetics; lipid-based nanoparticles

1. Introduction

Bisphosphonates, distinguished by their unique ‘P-C-P’ structure, are a class of phosphonate compounds clinically used to treat bone diseases such as osteoporosis (Drake et al., 2008; Russell et al., 2008). They also attract great attentions for bone tumor treatment, due to their ability to inhibit skeletal tumor growth, reduce tumor burden and cancer-induced bone diseases (e.g. bone pain, fracture) (Green, 2004; Heymann et al., 2004; Jimenez - Andrade et al., 2010; Ripamonti et al., 2009). Mechanistic studies have demonstrated that bisphosphonates can directly killing tumor cells, as well as have indirect antitumor effect by inhibiting or killing tumorassociated microphages (TAMs) in the tumor microenvironment (Gnant and Clézardin, 2012; Guise, 2008; Li et al., 2008; Rogers and Holen, 2011).

Recently, there is also interest in using bisphosphonates for extraskeletal tumor treatment (e.g. lung, breast, or prostate tumor) (Hillner et al., 2003; Oster et al., 2014; Rosen et al., 2003). Unfortunately, because of their unique pharmacokinetics profile (i.e. rapid elimination from plasma by renal clearance and extensive skeleton absorption), bisphosphonates usually have very limited distribution in extraskeletal tumors (Lin, 1996; Marra et al., 2009; Weiss et al., 2008). Several reformulating strategies have been applied to modify the pharmacokinetics and biodistribution of bisphosphonates. For instance, there are reports that encapsulating bisphosphonates (e.g. zoledronic acid (Zol), clodronic acid (Clo)) into functional liposomes causes significant changes in their tissue distribution, as well as an increase of bisphosphonate levels in tumors (Marra et al., 2011; Shmeeda et al., 2013; Zeisberger et al., 2006). Caraglia and colleagues have also developed an advanced Zol delivery system based on the self-assembly of calcium phosphate nanoparticles and cationic lipids, which significantly enhanced the accumulation of Zol in extraskeletal tumors (Marra et al., 2012; Salzano et al., 2011; Salzano et al., 2016).

Phosphonate-metal materials, including bisphosphonate-metal complexes, are materials that have extensive industrial applications (Alkordi et al., 2008; Clearfield and Demadis, 2011; García et al., 2012; Shimizu et al., 2013). However, the biomedical applications of such materials are still limited, probably related to the lack of studies on the control of their physical properties, such as morphology, size, dispersity, uniformity, hydrophilicity/

hydrophobicity, etc. (Shimizu et al., 2009; Zhu et al., 2014). Recently, Au and colleagues reported the utilization of a new reverse microemulsion (RM) method for the synthesis of DOPA (an anionic lipid)-coated bisphosphonate-metal composites (i.e. Zol-Ca@DOPA), which are small nano-spheres with good uniformity and monodispersity. Based on such Zol-Ca@DOPA composites, the authors developed a novel nanoparticle formulation for targeted delivery of Zol to subcutaneous tumors to explore the potential of using Zol to directly inhibit tumor cell growth (Au et al., 2016). Using nanoparticles prepared with fluorescently labeled cholesterol, the authors showed that surface-modification of the nanoparticles with folic acid increases their distribution in tumor tissues in a mouse model (Au et al., 2016). However, it remains unclear how such a nanoparticle formulation alters the biodistribution of Zol and whether it helps to reduce the distribution of Zol in bones. We sought to address these questions in the present study. We prepared a similar bisphosphonate-metal complex-based nanoparticle formulation by using Zol and calcium as the model bisphosphonate and metal molecules, respectively. The Zol-Ca@DOPA composites were prepared following the method by Au and colleagues (Au et al., 2016). DSPE-PEG_{2K} was utilized to wrap the highly lipophilic Zol-Ca@DOPA composites to facilitate their dispersion in an aqueous solution, and the resultant nanoparticle formulation was denoted as Zol-Ca@bi-lipid NPs. After further optimization and characterization, a type of Zol-Ca@bi-lipid NPs with single Zol-Ca@DOPA composite-based core was selected for further studies. The distribution and kinetics of Zol, free or in the Zol-Ca@bi-lipid NPs, in blood, bone, and major organs were evaluated and compared in a mouse model.

2. Materials and Methods

2.1 Reagents

Zoledronic acid monohydrate was from TCI America (Portland, OR). Alexa Fluor 647 (AF647)-labeled Zol (Zol-AF647) was from BioVinc LLC (Culver City, CA). Sodium hydrate, calcium chloride, sodium dihydrogen phosphate, sodium hydrogen phosphate, uranyl acetate (UA) dihydrate, formic acid and polyoxyethylene (5) nonylphenylether (NP-5) were from Sigma-Aldrich (St. Louis, MO). The 1, 2-dioleoyl-*sn*-glycero-3-phosphate monosodium salt (DOPA) and 1, 2-distearoyl-*sn*-glycero-3-phosphoethanolamine-N-[methoxy (polyethylene glycol)-2000 (DSPE-PEG_{2K}) were from Avanti Polar Lipid, Inc. (Alabaster, AL). Cyclohexane, dimethyl sulfoxide (DMSO), chloroform and ethanol were from Thermo Fisher Scientific Co. (Pittsburgh, PA). All reagents were used without further purification.

2.2 Animals

Female C57BL/6 mice (6–8 weeks) were from Charles River Laboratories (Wilmington, MA). Animal studies were performed in accordance with the National Research Council Guide for the Care and Use of Laboratory Animals. Animal protocol was approved by the Institutional Animal Care and Use Committee at The University of Texas at Austin.

2.3 Preparation and characterization of spherical Zol-Ca@DOPA composites using reverse microemulsion method

The spherical Zol-Ca@DOPA composites was prepared as previously described (Li et al., 2017). Briefly, the component ratios of V_{H2O}/V_{NP-5} and $V_{NP-5}/V_{cyclohexane}$ in RM were fixed at 1/13.3 and 30/70, respectively. To prepare the RM, 0.36 mL aqueous solution of reactant ($CaCl_2$ or Zol) was added into 16 mL mixture of NP-5 and cyclohexane. The concentrations of $CaCl_2$ or Zol in aqueous solution were 0.15 M and 0.02 M, respectively. To the Zol-containing RM, 0.24 mL DOPA solution (0.05 M in $CHCl_3$) was added dropwise to reach a final concentration of 0.9 mM. After sonication and then stirring for several minutes, this RM was mixed with the $CaCl_2$-containing RM. After overnight reaction, abundant ethanol was applied to break the RM. The white precipitate was collected, washed with ethanol twice, and dried. Thereafter, $CHCl_3$ was added to re-suspend the precipitate. The suspension obtained was passed through a 0.22 μm filter, dialyzed against $CHCl_3$ for 48 h in a benzoylated dialysis tube (2 KDa MWCO, Sigma-Aldrich), and stored in −20°C. Dynamic light scattering (DLS) and transmission electron microscope (TEM) were applied to determine the hydrodynamic particle size and morphology of the Zol-Ca@DOPA composites by using a Zetasizer Nano ZS (Malvern, Westborough, MA) and an FEI Tecnai TEM (available in the Institute for Cellular and Molecular Biology Microscopy and Imaging Facility at The University of Texas at Austin and operated with high tension of 80 kV), respectively.

2.4 Determination of Zol concentration by ionic exchange high performance liquid chromatography (IE-HLPC)

The concentration of Zol in the Zol-Ca@DOPA storage solution was determined by IE-HPLC (1260 Infinity II LC System from Agilent Technologies, Santa Clara, CA). Due to the hydrophobicity of Zol-Ca@DOPA composites, DSPE-PEG_{2k} was applied to suspend such composites in an aqueous solution. Typically, 0.1 mL Zol-Ca@DOPA suspension was added into a glass vial with 1 mg DSPE-PEG_{2k}, followed by the removal of $CHCl_3$. Thereafter, 1 mL IE-HPLC mobile phase (i.e. 0.2% formic acid with pH of ~3.0) was added into the glass vial followed by several minutes of water-bath sonication. The concentration of Zol in the solution was measured by IE-HPLC with an IC-Pak Anion HC column (4.6 × 150 mm and 10 μm, Waters Corp., Milford, MA), an absorption wavelength of 210 nm, and a flow rate of 1.8 mL/min.

2.5 Preparation and characterization of Zol-Ca@DOPA/DSPE-PEG_{2K} nanoparticle formulation (i.e. Zol-Ca@bi-lipid NPs)

To prepare Zol-Ca@bi-lipid NPs, a certain amount of Zol-Ca@DOPA composites together with DSPE-PEG_{2K} were suspended in 2 mL $CHCl_3$ to obtain a transparent solution. Thereafter, a thin film was formed after the removal of $CHCl_3$ using a rotary evaporator. The thin film was further applied to a CentriVap Benchtop Vacuum Concentrator (Labconco, Kansas City, MO) at 60 °C for 2 h before it was hydrated using 1 mL water (or 10 mM sodium phosphate buffer if needed) and sonicated for several minutes, followed by passing through a 0.45 μm filter and storing in 4 °C. The morphology of Zol-Ca@bi-lipid NPs was characterized using TEM. To prepare the specimen, 5 μL of Zol-Ca@bi-lipid NPs in

suspension was added onto a glow-discharge treated carbon-coated grid and allowed to dry. Thereafter, the specimen was observed directly or after negatively stained using 2% UA solution. The hydrodynamic size and zeta potential of such nanoparticles were measured using a Malvern Zetasizer Nano ZS. To determine the content of Zol in Zol-Ca@bi-lipid NPs, Zol-Ca@bi-lipid NPs in suspension were lyophilized and dissolved in 0.2% formic acid with pH ~3 before applying to IE-HPLC. The drug-loading efficiency (DLE) was the weight ratio of the Zol in the nanoparticles to the lyophilized nanoparticles. The recovery efficiency (RE) was the weight ratio of Zol detected in the Zol-Ca@bi-lipid NPs to the inputted amount of Zol in the Zol-Ca@DOPA hydrophobic core. The encapsulation efficiency (EE) was calculated using the amount of Zol in the Zol-Ca@bi-lipid preparations (calculated by subtracting free Zol in the preparations determined after ultrafiltration from inputted amount of Zol) divided by the total inputted amount of Zol. The preparations were not passed through a 0.45 μm filter when determining the EE. These experiments were repeated at least three times, and data reported are mean ± S.D.

2.6 In vitro release of Zol from Zol-Ca@bi-lipid NPs

The release of Zol from the Zol-Ca@bi-lipid NPs was determined by placing 1 mL of free Zol or Zol-Ca@bi-lipid NPs (Zol concentration, 0.6 mg/mL) into a dialysis tube (MWCO, 50 KDa, Spectrum Laboratories, Inc., Rancho Dominguez, CA), which was then placed into 9 mL of release medium (i.e. 10 mM sodium phosphate buffer, pH 5.0, 6.6, or 7.4) and incubated in a 37°C shaker incubator. At pre-designed time points, 1 mL of release medium was withdrawn and replaced with 1 mL fresh release medium. The concentration of Zol in the release medium was measured directly using IE-HPLC.

In the biodistribution study (see below), the Zol-Ca@bi-lipid NPs were made fluorescent by including Zol-AF647 (2%, w/w, of the total Zol). To understand the difference between the release profiles of Zol and Zol-AF647, we prepared Zol-Ca@bi-lipid NPs with Zol-AF647 (2%). Dialysis tubes with 0.4 mL of Zol-Ca@bi-lipid NPs in suspension were placed into 3.6 mL of release medium (i.e. 10 mM sodium phosphate buffer, pH 7.4) and incubated in a 37 °C shaker incubator. At pre-designed time points, 1 mL release medium was withdrawn and replaced with 1 mL fresh release medium. The samples were lyophilized and then re-dissolved in 0.1 mL mobile phase (i.e. 0.2% formic acid, pH ~3). The concentration of Zol in samples was measured using IE-HPLC as described above, and the concentration of Zol-AF647 in samples was measured using an UV spectrometer NanoDrop 2000 (Thermo Scientific, Wilmington, DE) at an absorption wavelength of 650 nm. For the release study, the experiments were repeated three times.

2.7 In vivo biodistribution of Zol-Ca@bi-lipid NPs in a mouse model

The biodistribution and kinetics of the Zol-Ca@bi-lipid NPs in blood, one of the hind legs, and various major organs were evaluated in C57BL/6 mice. Mice were intravenously injected with Zol-Ca@bi-lipid NPs, free Zol, or sterile PBS (as a control). The dose of Zol was 2 μg per mouse, and 2% (w/w) of the Zol was Zol-AF647. Mice (n = 3) were euthanized at various time points after injection (i.e. 0.5, 2.5, 6 or 24 h) to collect blood, right hind leg bone, and major organs (i.e. heart, lung, kidneys, pancreas, spleen and liver). All samples were then imaged using an IVIS Spectrum Imaging System (Caliper Life Sciences,

Waltham, MA) with excitation/emission wavelength of 640/680 nm, and the fluorescence intensities values were used as an indication of the distribution of the Zol. Data reported were normalized based on the values from the PBS group (i.e. the values of the PBS group were subtracted).

2.8 Statistical analysis

Data were analyzed using Student's t-test (i.e. unpaired) using the GraphPad Prism from GraphPad Software, Inc. (La Jolla, CA). Shaprio-Wilk normality test of data, including those from a preliminary study, showed that the zoledronic acid (in vivo biodistribution) data follow normal distribution. A p value of ≤ 0.05 (two-tailed) is considered significant.

3. Results and Discussion

3.1 Preparation and Characterization of Zol-Ca@bi-lipid NPs

Fig. 1A shows a representative TEM image of the DOPA-coated Zol-Ca composites (Zol-Ca@DOPA). These composites are spherical, around 15 nm, monodispersed, and uniform. The relative number hydrodynamic size distribution of the Zol-Ca@DOPA composites is shown in Fig. 1B. Their average hydrodynamic size is 14.8 ± 2.3 nm, which is in agreement with the particle size estimated using the TEM image.

Due to the hydrophobicity of Zol-Ca@DOPA composites, DSPE-PEG_{2K} was used to wrap such composites to enable their suspension in an aqueous solution to form nanoparticles (i.e. Zol-Ca@bi-lipid NPs). Fig. 2 shows the effect of the inputted weight ratio of Zol-Ca@DOPA composites (i.e. amount of Zol) and DSPE-PEG_{2K} on certain physical properties of the resultant Zol-Ca@bi-lipid NPs. When the Zol/DSPE-PEG_{2K} ratio was increased from 15 μg/mg to 120 μg/mg, the drug (i.e. Zol) loading efficiency (DLE) increased from 1.6% to 4.2%, and as expected, the encapsulation efficiency (EE) of Zol decreased from 93.6 ± 0.4% to 78.8 ± 3.3% (Fig. 2A). Moreover, the recovery efficiency (RE) of Zol was around 80% in the Zol-Ca@bi-lipid NPs prepared with a Zol/DSPE-PEG_{2K} ratio of 30 μg/mg or less, but decreased sharply when the Zol/DSPE-PEG_{2K} ratio was higher than 30 μg/mg (e.g. 60 to 120 μg/mg) (Fig. 2B), likely due to the difficulty in the formation of small, monodispersed Zol-Ca@bi-lipid NPs at high Zol/DSPE-PEG_{2K} ratios; a significant portion of the preparations was likely lost when the samples were applied to a 0.45 μm filter. The mean hydrodynamic size of the resultant Zol-Ca@bi-lipid NPs increased from 12.5 nm to 92.5 nm with the polydispersity index (PDI) decreased from 0.41 to around 0.2 (Fig. 2C). Furthermore, the zeta potential of the resultant Zol-Ca@bi-lipid NPs increased from −27.4 ± 1.2 mV to −8.9 ± 1.5 mV (Fig. 2D).

Clearly, increasing the weight ratio of Zol-Ca@DOPA to DSPE-PEG_{2k} led to an increase in the size of the resultant nanoparticles. Given that the mean diameter of the Zol-Ca@DOPA composites was only ~15 nm (Fig. 1), it is likely that the Zol-Ca@bi-lipid NPs with slightly larger size (e.g. > 15 nm and < 30 nm) have an inner core consisting of single Zol-Ca@DOPA composite, whereas larger nanoparticles (e.g. > 30 nm) may contain multiple Zol-Ca@DOPA composites. For example, when the Zol/DSPE-PEG_{2K} ratio was 15 or 20 μg/mg, the majority of the Zol-Ca@bi-lipid NPs formed appeared to be small with a single

Zol-Ca@DOPA composite inner core (Fig. 2E). In contrast, when the Zol/DSPE-PEG_{2K} ratio was increased to 60 or 120 μg/mg, the resultant Zol-Ca@bi-lipid NPs were much larger and contained multiple Zol-Ca@DOPA composites (Fig. 2E), likely because the amount of DSPE-PEG_{2k} added was not enough to wrap the outer surface of every single Zol-Ca@DOPA composite anymore.

Based on the above results, the Zol-Ca@bi-lipid NPs that were prepared with a Zol/DSPE-PEG_{2K} weight ratio of 20 μg/mg were selected for further studies, because almost all the resultant nanoparticles had a single Zol-Ca@DOPA composite core (Fig. 2E), and such Zol-Ca@bi-lipid NPs had high Zol encapsulation efficiency (i.e. 92.1 ± 1.3%), high Zol recovery efficiency (i.e. 78.3 ± 1.2%), and small particle size of 23.6 ± 1.8 nm with low polydispersity index (i.e. ~0.2). Fig. 3A shows a representative TEM image of the Zol-Ca@bi-lipid NPs after negative staining. The diameter of such nanoparticles based on the TEM images is estimated to be ~25 nm, which is in agreement with the mean hydrodynamic size measured using DLS (histogram of distribution by number shown in Fig. 3B). The TEM images also showed that the Zol-Ca@bi-lipid nanoparticles appeared to have a core (i.e. Zol-Ca@DOPA composite) and a lipid layer-based shell structure.

3.2 pH-responsive drug release of Zol-Ca@bi-lipid NPs

The release profiles of Zol from the Zol-Ca@bi-lipid NPs were determined in normal physiological pH (i.e. pH 7.4) and lower pH values (i.e. pH 6.8 and 5.0), because data from previous studies indicated that the release of Zol from Zol-Ca complexes is pH dependent (Au et al., 2016; Liu et al., 2012). As shown in Fig. 4, the release rate of Zol from Zol-Ca@bi-lipid NPs was higher in lower pH. For example, after 48 h, only about 35% of Zol was released from the nanoparticles at pH 7.4, in comparison to ~45% at pH 6.8 and ~75% at 5.0. This finding confirmed that the release of Zol from the Zol-Ca@bi-lipid NPs is pH-sensitive, likely because the high concentration of protons in lower pH more effectively disrupt the chemical interactions between the phosphate anions and calcium cations in the Zol-Ca complexes (Dorozhkin, 2012). The pH-dependent release of Zol from the Zol-Ca@bi-lipid NPs will likely be beneficial for future application of the Zol-Ca@bi-lipid NPs in tumor therapy as the pH in tumor microenvironment is known to be lower than normal physiological pH (Helmlinger et al., 1997; Parolini et al., 2009). It is expected that the Zol-Ca@bi-lipid NPs will likely have limited Zol release when circulating in blood, and then release more Zol when reach tumor tissues.

In addition, it is noted that there is a disagreement about the release of Zol from Zol-Ca complexes in normal physiological pH (i.e. pH 7.4) in the literature. For instance, Liu et al., (2012) reported that in 5 mM phosphate-buffered saline (PBS), more than 30% of Zol was released from bare or lipid-coated Zol-Ca rods within 24 h, which agrees with our result shown in Fig. 4. However, Au et al. (2016) reported that their Zol-Ca/lipid nanoparticle formulation was fairly stable and only release less than 5% of Zol in a pH 7 phosphate buffer (100 mM) after 24 h. We also noticed that the release of Zol from our Zol-Ca@bi-lipid NPs was much slower in a 50 mM phosphate buffer (data not shown). Our Zol-Ca@bi-lipid NPs are similar to the nanoparticles reported by Au et al. (2016). We speculate that high concentrations of phosphate anions may significantly slow down the release of Zol from the

Zol-Ca complexes. This phenomenon is probably related to the release of Ca^{2+} together with the release of Zol from Zol-Ca complexes in aqueous solution. Since there are hydrogen phosphate anions (i.e. HPO_4^{2-}) in the release medium, they may interact with Ca^{2+} to form $CaHPO_4$ precipitates (Newton and Driscoll, 2008). When the concentration of HPO_4^{2-} is high (e.g. in 0.05 – 0.1 M phosphate buffers), more insoluble $CaHPO_4$ may form and deposit on the outer surface of nanoparticles, thus blocking further dissociation of the Zol-Ca complexes (i.e. the release of Zol). Given that the concentration of phosphate anions in normal physiological condition is relatively low (i.e. 5 to 10 mM) (Hugentobler et al., 2007; Kestenbaum et al., 2005), it is therefore expected that our Zol-Ca@bi-lipid NPs will release some Zol when circulating in blood after i.v. injection.

3.3 In vivo pharmacokinetics and distribution of Zol in Zol-Ca@bi-lipid NPs

In order to investigate if our Zol-Ca@bi-lipid NPs could modulate the biodistribution and pharmacokinetics of Zol, we studied the plasma and tissue kinetics of Zol in Zol-Ca@bi-lipid NPs and compared them to that of free Zol in a mouse model. To readily detect Zol, 2% (w/w) of the Zol was the fluorescently labeled Zol-AF647. It has been reported that free bisphosphonates and their relative fluorescently labeled bisphosphonates, including Zol and Zol-AF647, have very similar in vivo distributions (Junankar et al., 2015; Roelofs et al., 2012; Sun et al., 2015). C57BL/6 mice were i.v. injected with Zol-Ca@bi-lipid NPs or free Zol, both containing 2% of Zol-AF647, and mice were euthanized at different time points after injection to collect blood, right hind leg bone, and major organs, and the contents of Zol in them were determined by measuring the fluorescence intensity values.

Shown in Fig. 5A are the blood Zol concentration vs. time curves. Free Zol underwent rapid clearance after i.v. injection, whereas the Zol-Ca@bi-lipid NPs significantly slowed down the clearance of Zol (e.g. ~3.6-fold decrease in observed clearance (Cl_{obs}), ~3.6-fold increase in $AUC_{0\text{-}inf}$) (data based on PKSolver, non-compartment i.v. bonus model (Zhang et al., 2010)). Importantly, the Zol-Ca@bi-lipid NPs significantly decreased Zol distribution in mouse leg bone, as compared to free Zol (Fig. 5B). The fluorescent images of the bones and other major organs taken from the mice 24 h after i.v. injection of free Zol or the Zol-Ca@bi-lipid NPs are shown in Fig. 5C. The fluorescent images of bones and other major organs taken at other time points, including in mice injected with sterile PBS as a control, are shown in Fig. S1–S4. Bisphosphonates (e.g. Zol) have demonstrated clinical efficacy against skeletal tumors (Green, 2004; Heymann et al., 2004). However, due to their preferred accumulation in bones, bisphosphonates have no or only limited activity against extraskeletal tumors (Marra et al., 2009; Weiss et al., 2008). Moreover, it is known that certain side effects of bisphosphonates, e.g. jaw necrosis, are tightly related to their accumulation in bones as well (Ruggiero et al., 2004; Woo et al., 2006). Therefore, our finding that formulating Zol into Zol-Ca@bi-lipid NPs decreases the bone distribution of Zol suggest that they can be potentially applied to treat extraskeletal tumors, as well as minimize their side effects. It is noted that although at a relatively lower level, Zol distribution in bones remained significant even after i.v. inject ion of the Zol-Ca@bi-lipid NPs (Fig. 5B–C). This is likely related to the release of Zol from the nanoparticles when circulating in blood. Future effort of minimizing the release of Zol from similar

nanoparticles in blood circulation is expected to further help reduce or minimize its bone distribution.

In major organs, there were significant differences in the fluorescence intensity values in the kidneys (at the 0.5 h time point), spleen, liver (Fig. 5C–E), but not in heart, lung or pancreas (Fig. S5) of mice i.v. injected with Zol-Ca@bi-lipid NPs or free Zol. As expected, when injected with free Zol, fluorescent signal can be detected in mouse kidneys at early time point (i.e. 0.5 h), likely because Zol is normally cleared from the kidneys (Lin, 1996; Lin et al., 1991). As to mice injected with the Zol-Ca@bi-lipid NPs, fluorescent signals were significantly higher in their liver and spleen, as compared to that in mice injected with free Zol (Figs. 5D–E). This may be attributed to the particulate nature of the Zol-Ca@bi-lipid NPs, which facilitates their distribution in the mononuclear phagocyte system (e.g. liver and spleen) (Albanese et al., 2012; Storm et al., 1995).

Taken together, data in Fig. 5 indicate that the Zol-Ca@bi-lipid NPs significantly modify the blood and tissue distribution and kinetics of Zol in a mouse model. In the present in vivo study, a small percent of the Zol used was Zol-AF647, which enables the quantitation of the Zol in the blood, bone and major organs of mice by ex-vivo fluorescence imaging. Data from previous studies showed that fluorescently labeled bisphosphonates, e.g. Zol-AF647, mainly accumulate in bones, which is similar to their unlabeled parent bisphosphonates (Junankar et al., 2015; Roelofs et al., 2012; Sun et al., 2015). However, conjugating AF647 onto Zol affects its physicochemical properties. In order to verify the feasibility of using the Zol-AF647 as the fluorescent probe to study the pharmacokinetics and biodistribution of unlabeled Zol delivered by the Zol-Ca@bi-lipid NPs, the release profile of Zol-AF647 from such nanoparticles prepared with 2% of Zol-AF647 was evaluated and compared to the release profile of the free, unlabeled Zol from the same nanoparticles. As shown in Fig. 6, the rate at which the Zol-AF647 is released from the Zol-Ca@bi-lipid NPs (with 2% Zol-AF647) is similar to (or not higher than) that of the unlabeled Zol from the same nanoparticles, indicating that the pharmacokinetics and biodistribution data generated by measuring Zol-AF647 (Fig. 5) are indicative of the pharmacokinetics and biodistribution of the unlabeled Zol in the Zol-Ca@bi-lipid NPs.

As mentioned earlier, there is increasing interest in developing new formulations to alter the in vivo biodistribution of bisphosphonates, and thus enhance their applications in extraskeletal tumor therapy (Oster et al., 2014; Rosen et al., 2003). Most of the reported formulations, such as the bisphosphonate-encapsulated liposomes (e.g. liposomal Zol or Col) and the Zol-embedded pre-formed calcium phosphate and cationic lipids hybrid nanoparticles, have been shown to be able to change the biodistribution of the bisphosphonates (Marra et al., 2012; Salzano et al., 2011; Salzano et al., 2016; Shmeeda et al., 2013). Compared to those formulations, the delivery systems based on the bisphosphonate-metal complexes recently reported by Au and colleagues offer an alternative platform: spherical Zol-Ca complexes were prepared using a RM technique, and the complexes were then coated with folic acid-modified lipids for targeted delivery of Zol into subcutaneous tumors in a mouse model (Au et al., 2016). However, in their in vivo biodistribution study, fluorescently labeled cholesterol compounds were used to show that the folic acid on the nanoparticles was able to help increase the distribution of the

nanoparticles into tumor tissues, as compared to nanoparticles that were not modified with folic acid (Au et al., 2016). In other words, the authors did not report the distribution of Zol in tumor tissues, nor in mouse bones. Our data showed that the distributions of Zol in mouse bone and some major organs were significantly modified by the Zol-Ca@bi-lipid NPs, as compared to free Zol, thus helping lay the foundation for exploring the application of formulations based on complexes formed by direct bisphosphonate-metal interactions for extraskeletal tumor therapy.

4. Conclusions

In the present study, we showed that a Zol-nanoparticle formulation prepared using Zol-Ca nanocomposites synthesized by a reverse microemulsion method reduces the bone distribution of Zol, decreases its clearance rate in blood, and alters its tissue distribution. It is expected that similar bisphosphonate-metal material-based nanoparticle formulations can be applied to help reduces the side effects of bisphosphonates and expand their applications in extraskeletal tissues.

Supplementary Material

Refer to Web version on PubMed Central for supplementary material.

Acknowledgments

This work is supported in part by a U.S. National Institutes of Health grant (CA135274 to Z.C.). Z.C is also supported by the National Natural Science Foundation of China (81460454) and the Inner Mongolia Natural Science Fund (2014ZD05).

References

Albanese A, Tang PS, Chan WC. The effect of nanoparticle size, shape, and surface chemistry on biological systems. Annual review of biomedical engineering. 2012; 14:1–16.

Alkordi MH, Liu Y, Larsen RW, Eubank JF, Eddaoudi M. Zeolite-like metal-organic frameworks as platforms for applications: on metalloporphyrin-based catalysts. Journal of the American Chemical Society. 2008; 130:12639–12641. [PubMed: 18759392]

Au KM, Satterlee A, Min Y, Tian X, Kim YS, Caster JM, Zhang L, Zhang T, Huang L, Wang AZ. Folate-targeted pH-responsive calcium zoledronate nanoscale metal-organic frameworks: Turning a bone antiresorptive agent into an anticancer therapeutic. Biomaterials. 2016; 82:178–193. [PubMed: 26763733]

Clearfield, A. The early history and growth of metal phosphonate chemistry. In Metal Phosphonate Chemistry: from synthesis to applications. In: Clearfield, A., Demadis, K., editors. R Soc Chem. 2011. p. 1-44.

Dorozhkin SV. Dissolution mechanism of calcium apatites in acids: A review of literature. World journal of methodology. 2012; 2:1–17. [PubMed: 25237611]

Drake MT, Clarke BL, Khosla S. Bisphosphonates: mechanism of action and role in clinical practice, Mayo Clinic Proceedings. Elsevier. 2008:1032–1045.

García EJ, Mowat JP, Wright PA, Pérez-Pellitero J, Jallut C, Pirngruber GD. Role of structure and chemistry in controlling separations of CO2/CH4 and CO2/CH4/CO mixtures over honeycomb MOFs with coordinatively unsaturated metal sites. The Journal of Physical Chemistry C. 2012; 116:26636–26648.

Gnant M, Clézardin P. Direct and indirect anticancer activity of bisphosphonates: a brief review of published literature. Cancer treatment reviews. 2012; 38:407–415. [PubMed: 21983264]

Green JR. Bisphosphonates: preclinical review. The Oncologist. 2004; 9:3–13.

Guise TA. Antitumor effects of bisphosphonates: promising preclinical evidence. Cancer treatment reviews. 2008; 34:S19–S24. [PubMed: 18486348]

Helmlinger G, Yuan F, Dellian M, Jain RK. Interstitial pH and pO_2 gradients in solid tumors in vivo: high-resolution measurements reveal a lack of correlation. Nature medicine. 1997; 3:177–182.

Heymann D, Ory B, Gouin F, Green JR, Redini F. Bisphosphonates: new therapeutic agents for the treatment of bone tumors. Trends in molecular medicine. 2004; 10:337–343. [PubMed: 15242682]

Hillner BE, Ingle JN, Chlebowski RT, Gralow J, Yee GC, Janjan NA, Cauley JA, Blumenstein BA, Albain KS, Lipton A. American Society of Clinical Oncology 2003 update on the role of bisphosphonates and bone health issues in women with breast cancer. Journal of Clinical Oncology. 2003; 21:4042–4057. [PubMed: 12963702]

Hugentobler S, Morris D, Sreenan J, Diskin M. Ion concentrations in oviduct and uterine fluid and blood serum during the estrous cycle in the bovine. Theriogenology. 2007; 68:538–548. [PubMed: 17617447]

Jimenez-Andrade JM, Mantyh WG, Bloom AP, Ferng AS, Geffre CP, Mantyh PW. Bone cancer pain. Annals of the New York Academy of Sciences. 2010; 1198:173–181. [PubMed: 20536932]

Junankar S, Shay G, Jurczyluk J, Ali N, Down J, Pocock N, Parker A, Nguyen A, Sun S, Kashemirov B. Real-time intravital imaging establishes tumor-associated macrophages as the extraskeletal target of bisphosphonate action in cancer. Cancer discovery. 2015; 5:35–42. [PubMed: 25312016]

Kestenbaum B, Sampson JN, Rudser KD, Patterson DJ, Seliger SL, Young B, Sherrard DJ, Andress DL. Serum phosphate levels and mortality risk among people with chronic kidney disease. Journal of the American Society of Nephrology. 2005; 16:520–528. [PubMed: 15615819]

Li X, Naguib Y, Valdes S, Hufnagel S, Cui Z. Reverse microemulsion-based synthesis of (bis) phosphonate-metal materials with controllable physical properties: an example using zoledronic acid-calcium complexes. ACS applied materials & interfaces. 2017; 9:14478–14489. [PubMed: 28252282]

Li Y-Y, Chang JW-C, Chou W-C, Liaw C-C, Wang H-M, Huang J-S, Wang C-H, Yeh K-Y. Zoledronic acid is unable to induce apoptosis, but slows tumor growth and prolongs survival for non-small-cell lung cancers. Lung Cancer. 2008; 59:180–191. [PubMed: 17900752]

Lin J. Bisphosphonates: a review of their pharmacokinetic properties. Bone. 1996; 18:75–85. [PubMed: 8833200]

Lin J, Duggan D, Chen I-W, Ellsworth R. Physiological disposition of alendronate, a potent anti-osteolytic bisphosphonate, in laboratory animals. Drug Metabolism and Disposition. 1991; 19:926–932. [PubMed: 1686238]

Liu D, Kramer SA, Huxford-Phillips RC, Wang S, Della Rocca J, Lin W. Coercing bisphosphonates to kill cancer cells with nanoscale coordination polymers. Chemical Communications. 2012; 48:2668–2670. [PubMed: 22428170]

Marra M, Abbruzzese A, Addeo R, Prete S, Tassone P, Tonini G, Tagliaferri P, Santini D, Caraglia M. Cutting the limits of aminobisphosphonates: new strategies for the potentiation of their anti-tumour effects. Current cancer drug targets. 2009; 9:791–800. [PubMed: 20025567]

Marra M, Salzano G, Leonetti C, Porru M, Franco R, Zappavigna S, Liguori G, Botti G, Chieffi P, Lamberti M. New self-assembly nanoparticles and stealth liposomes for the delivery of zoledronic acid: a comparative study. Biotechnology advances. 2012; 30:302–309. [PubMed: 21741464]

Marra M, Salzano G, Leonetti C, Tassone P, Scarsella M, Zappavigna S, Calimeri T, Franco R, Liguori G, Cigliana G. Nanotechnologies to use bisphosphonates as potent anticancer agents: the effects of zoledronic acid encapsulated into liposomes. Nanomedicine: Nanotechnology, Biology and Medicine. 2011; 7:955–964.

Newton DW, Driscoll DF. Calcium and phosphate compatibility: revisited again. American Journal of Health-System Pharmacy. 2008; 65:73–80. [PubMed: 18159044]

Oster G, Lamerato L, Glass AG, Richert-Boe KE, Lopez A, Chung K, Richhariya A, Dodge T, Wolff GG, Balakumaran A. Use of intravenous bisphosphonates in patients with breast, lung, or prostate cancer and metastases to bone: a 15-year study in two large US health systems. Supportive Care in Cancer. 2014; 22:1363–1373. [PubMed: 24389827]

Parolini I, Federici C, Raggi C, Lugini L, Palleschi S, De Milito A, Coscia C, Iessi E, Logozzi M, Molinari A. Microenvironmental pH is a key factor for exosome traffic in tumor cells. Journal of Biological Chemistry. 2009; 284:34211–34222. [PubMed: 19801663]

Ripamonti C, Maniezzo M, Campa T, Fagnoni E, Brunelli C, Saibene G, Bareggi C, Ascani L, Cislaghi E. Decreased occurrence of osteonecrosis of the jaw after implementation of dental preventive measures in solid tumour patients with bone metastases treated with bisphosphonates. The experience of the National Cancer Institute of Milan. Annals of Oncology. 2009; 20:137–145.

Roelofs AJ, Stewart CA, Sun S, Błażewska KM, Kashemirov BA, McKenna CE, Russell RGG, Rogers MJ, Lundy MW, Ebetino FH. Influence of bone affinity on the skeletal distribution of fluorescently labeled bisphosphonates in vivo. Journal of Bone and Mineral Research. 2012; 27:835–847. [PubMed: 22228189]

Rogers TL, Holen I. Tumour macrophages as potential targets of bisphosphonates. Journal of translational medicine. 2011; 9:117–134. [PubMed: 21777410]

Rosen LS, Gordon D, Tchekmedyian S, Yanagihara R, Hirsh V, Krzakowski M, Pawlicki M, de Souza P, Zheng M, Urbanowitz G. Zoledronic acid versus placebo in the treatment of skeletal metastases in patients with lung cancer and other solid tumors: a phase III, double-blind, randomized trial—the Zoledronic Acid Lung Cancer and Other Solid Tumors Study Group. Journal of Clinical Oncology. 2003; 21:3150–3157. [PubMed: 12915606]

Ruggiero SL, Mehrotra B, Rosenberg TJ, Engroff SL. Osteonecrosis of the jaws associated with the use of bisphosphonates: a review of 63 cases. Journal of oral and maxillofacial surgery. 2004; 62:527–534. [PubMed: 15122554]

Russell R, Watts N, Ebetino F, Rogers M. Mechanisms of action of bisphosphonates: similarities and differences and their potential influence on clinical efficacy. Osteoporosis international. 2008; 19:733–759. [PubMed: 18214569]

Salzano G, Marra M, Porru M, Zappavigna S, Abbruzzese A, La Rotonda M, Leonetti C, Caraglia M, De Rosa G. Self-assembly nanoparticles for the delivery of bisphosphonates into tumors. International journal of pharmaceutics. 2011; 403:292–297. [PubMed: 21055454]

Salzano G, Zappavigna S, Luce A, D'Onofrio N, Balestrieri M, Grimaldi A, Lusa S, Ingrosso D, Artuso S, Porru M. Transferrin-Targeted Nanoparticles Containing Zoledronic Acid as a Potential Tool to Inhibit Glioblastoma Growth. Journal of Biomedical Nanotechnology. 2016; 12:811–830. [PubMed: 27301207]

Shimizu GK, Taylor JM, Kim S. Proton conduction with metal-organic frameworks. Science. 2013; 341:354–355. [PubMed: 23888028]

Shimizu GK, Vaidhyanathan R, Taylor JM. Phosphonate and sulfonate metal organic frameworks. Chemical Society Reviews. 2009; 38:1430–1449. [PubMed: 19384446]

Shmeeda H, Amitay Y, Tzemach D, Gorin J, Gabizon A. Liposome encapsulation of zoledronic acid results in major changes in tissue distribution and increase in toxicity. Journal of Controlled Release. 2013; 167:265–275. [PubMed: 23419948]

Storm G, Belliot SO, Daemen T, Lasic DD. Surface modification of nanoparticles to oppose uptake by the mononuclear phagocyte system. Advanced drug delivery reviews. 1995; 17:31–48.

Sun S, Błażewska KM, Kadina AP, Kashemirov BA, Duan X, Triffitt JT, Dunford JE, Russell RGG, Ebetino FH, Roelofs AJ. Fluorescent bisphosphonate and carboxyphosphonate probes: a versatile imaging toolkit for applications in bone biology and biomedicine. Bioconjugate chemistry. 2015; 27:329–340. [PubMed: 26646666]

Weiss HM, Pfaar U, Schweitzer A, Wiegand H, Skerjanec A, Schran H. Biodistribution and plasma protein binding of zoledronic acid. Drug Metabolism and Disposition. 2008; 36:2043–2049. [PubMed: 18625688]

Woo S-B, Hellstein JW, Kalmar JR. Systematic review: bisphosphonates and osteonecrosis of the jaws. Annals of internal medicine. 2006; 144:753–761. [PubMed: 16702591]

Zeisberger S, Odermatt B, Marty C, Zehnder-Fjällman A, Ballmer-Hofer K, Schwendener R. Clodronate-liposome-mediated depletion of tumour-associated macrophages: a new and highly effective antiangiogenic therapy approach. British journal of cancer. 2006; 95:272–281. [PubMed: 16832418]

Zhang Y, Huo M, Zhou J, Xie S. PKSolver: An add-in program for pharmacokinetic and pharmacodynamic data analysis in Microsoft Excel. Computer methods and programs in biomedicine. 2010; 99:306–314. [PubMed: 20176408]

Zhu Y-P, Ma T-Y, Liu Y-L, Ren T-Z, Yuan Z-Y. Metal phosphonate hybrid materials: from densely layered to hierarchically nanoporous structures. Inorganic Chemistry Frontiers. 2014; 1:360–383.

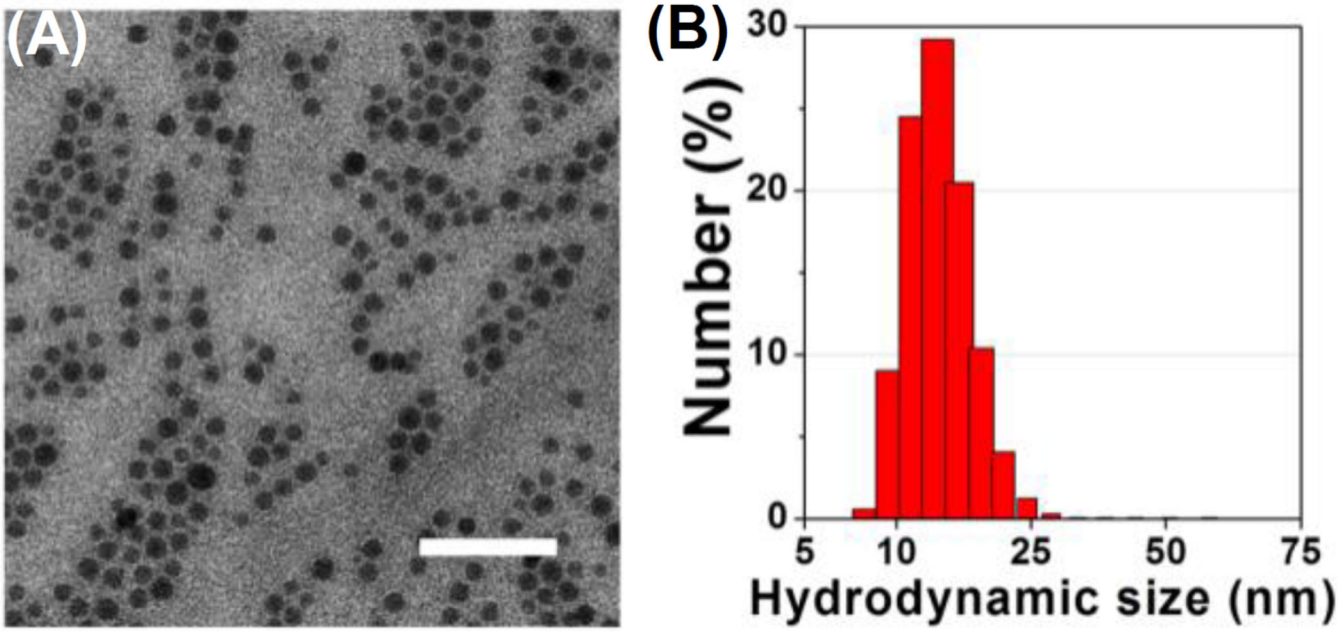

Fig. 1.

(A) A representative TEM image of DOPA-coated zoledronic acid-calcium (Zol-Ca@DOPA) composites (bar = 100 nm); **(B)** the hydrodynamic size distribution of the Zol-Ca@DOPA (in $CHCl_3$).

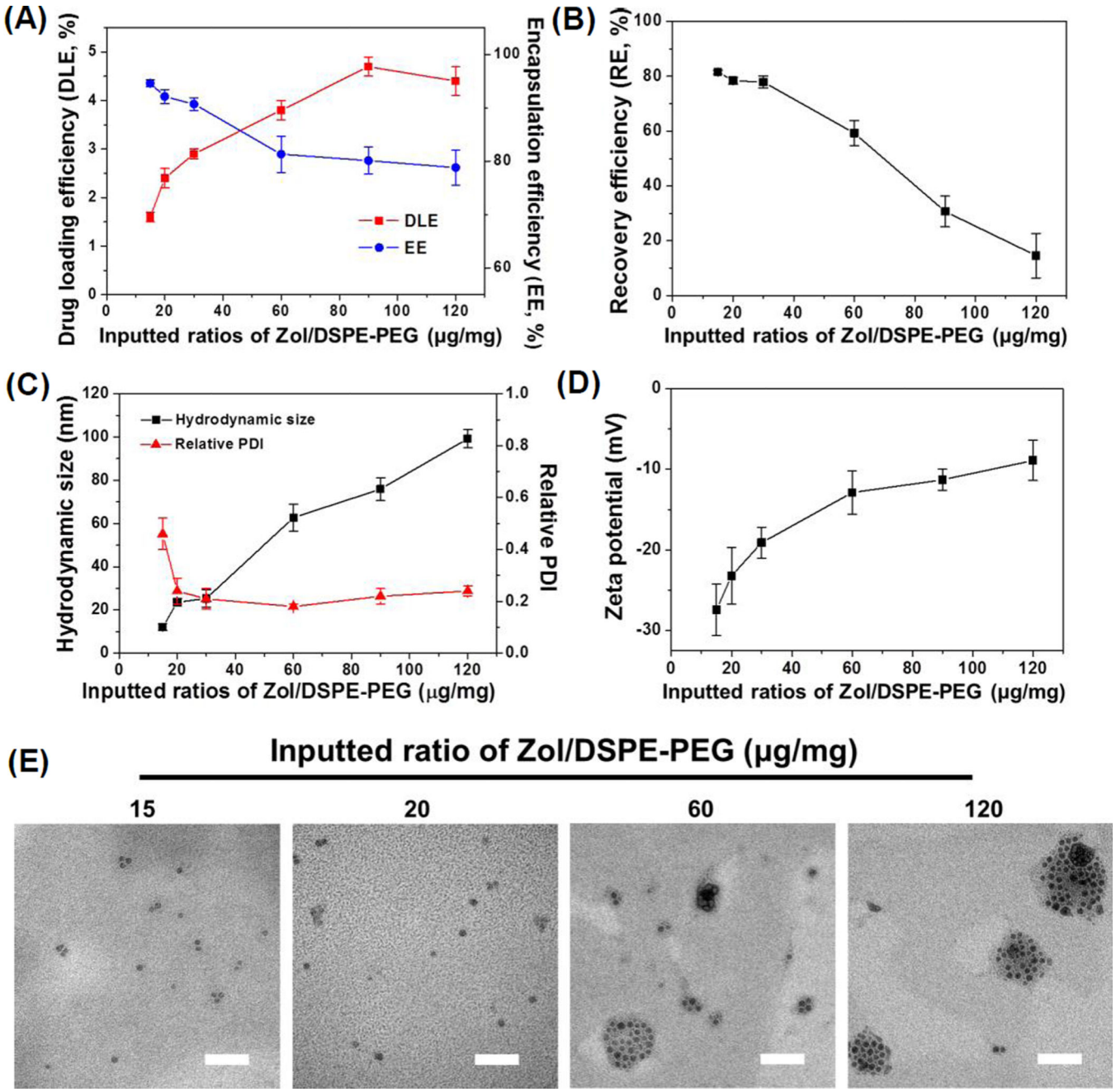

Fig. 2.

The effect of the ratio of Zol-Ca@DOPA to DSPE-PEG_{2k} (i.e. Zol/DSPE-PEG_{2k}) on the drug (Zol) loading efficiency (DLE) and encapsulation efficiency (EE) of Zol **(A)**, recovery efficiency (RE) of Zol **(B)**, average hydrodynamic size (by number) and polydispersity index (PDI) **(C)**, and zeta potential **(D)** of the resultant Zol-Ca@bi-lipid NPs. **(E)** Representative TEM images of Zol-Ca@bi-lipid NPs prepared with different Zol/DSPE-PEG_{2k} ratios (i.e. 15, 20, 60 and 120 μg/1 mg) (bar = 100 nm). In A–D, data shown are mean ± S.D. ($n \geq 3$).

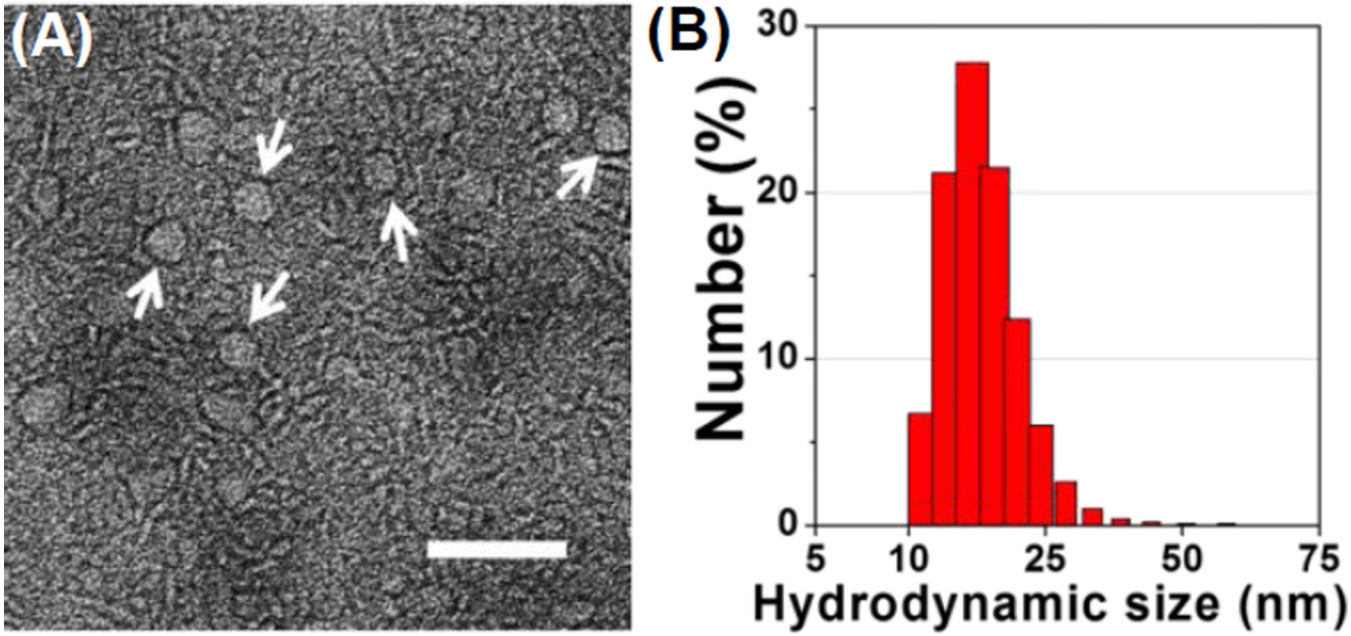

Fig. 3.

Characterization of Zol-Ca@bi-lipid NPs prepared with a Zol-Ca@DOPA to DSPE-PEG_{2k} ratio of 20 μg/1 mg. **(A)** a representative TEM image after negative staining. Nanoparticles with clear core-shell structure are indicated by white arrows (bar = 100 nm); **(B)** hydrodynamic size distribution of the Zol-Ca@bi-lipid NPs in aqueous suspension.

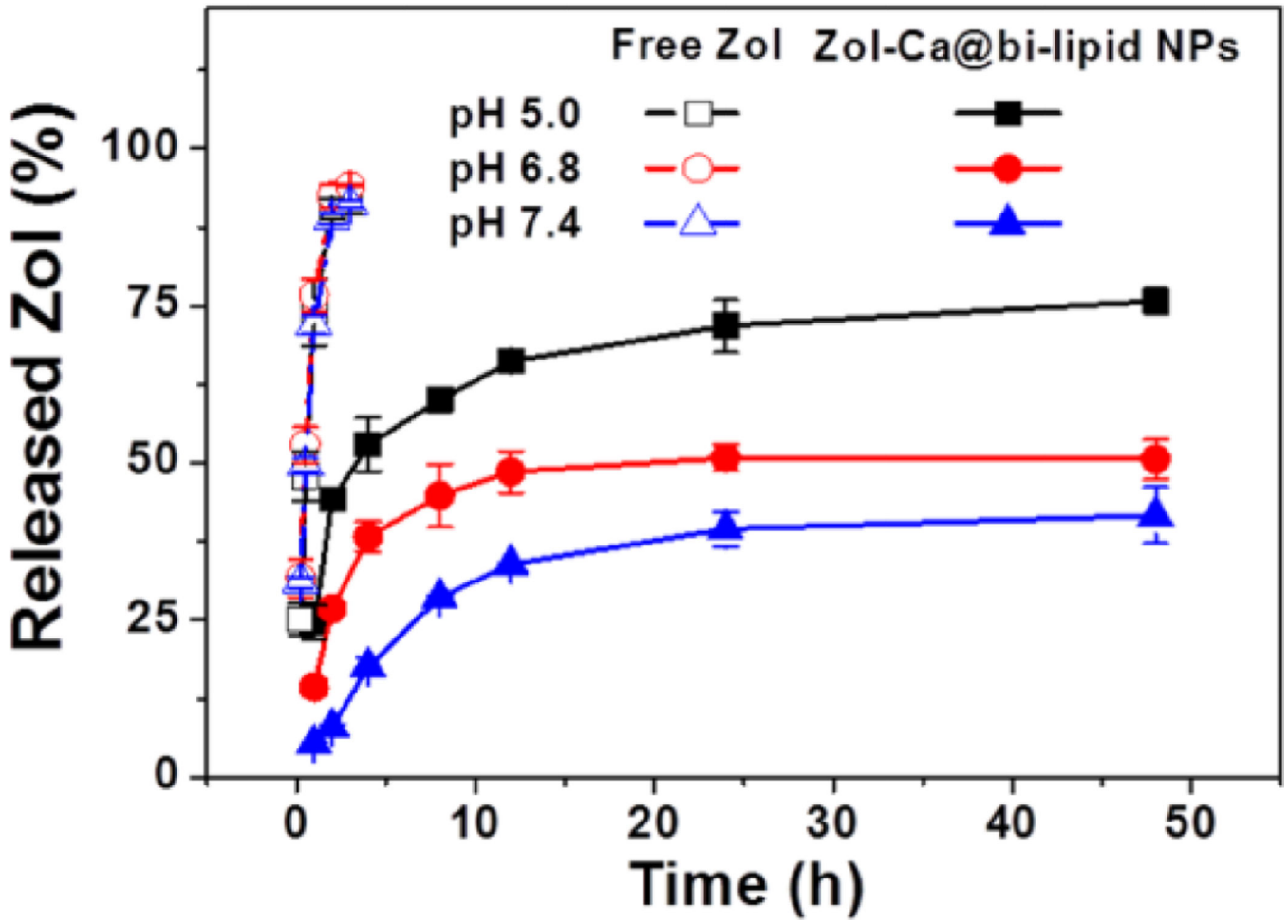

Fig. 4.

The release profiles of Zol from Zol-Ca@bi-lipid NPs in 10 mM sodium phosphate buffers with different pH values (i.e. 5.0, 6.8 and 7.4). As controls, the diffusion of free Zol across the dialysis member was also measured at different pH values. Data are mean ± S.D. (n = 3).

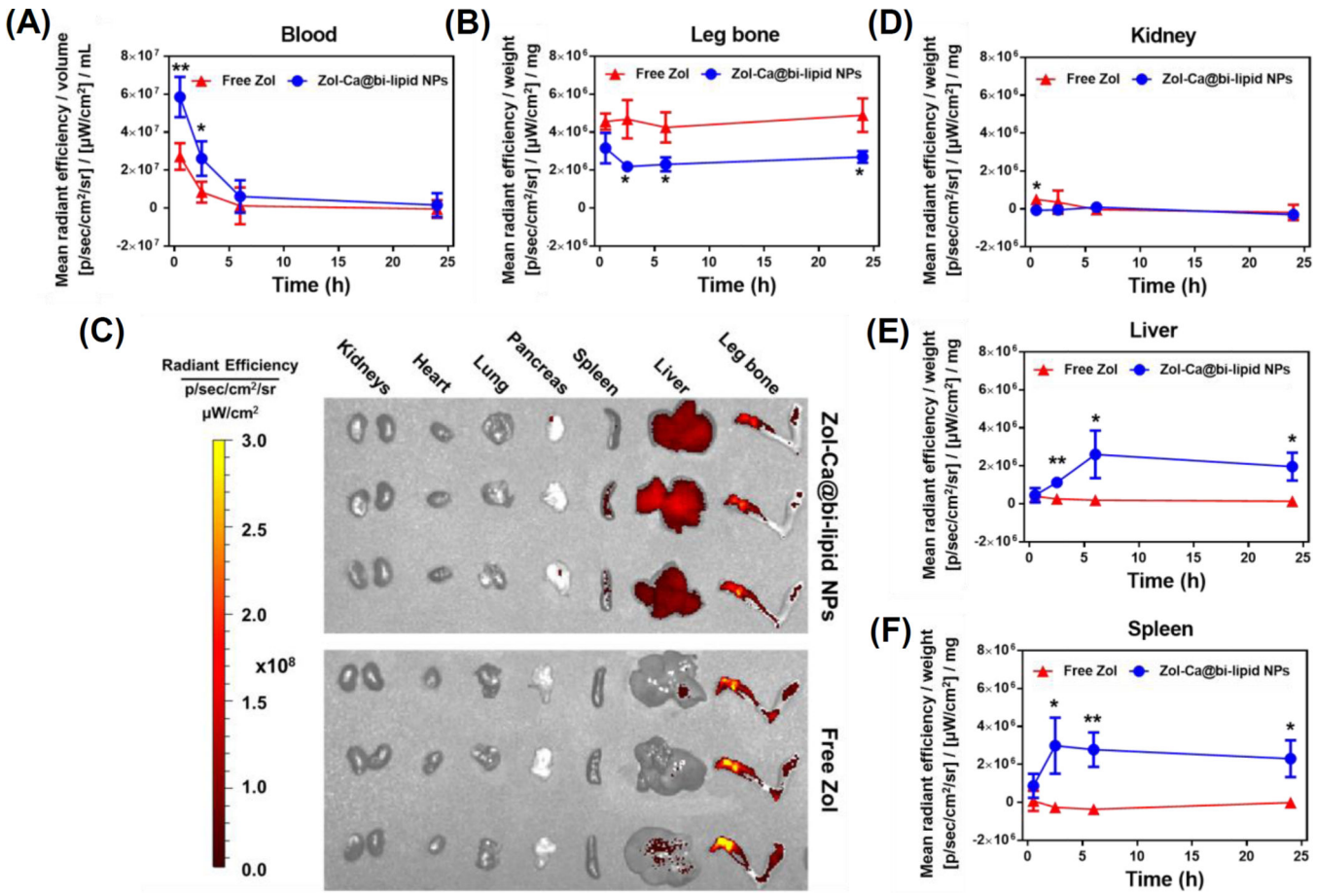

Fig. 5.

Blood and tissue pharmacokinetics of Zol in Zol-Ca@bi-lipid NPs. Mice were i.v. injected with Zol-Ca@bi-lipid NPs or free Zol with an equivalent amount of Zol (with 2% Zol-AF647) and euthanized 0.5, 2.5, 6 or 24 h after injection. Fluorescence intensity in blood, right hind leg bone, and major organs were measured. The results are expressed as values after subtracting mean values from the PBS group. **(A)** Blood, **(B)** leg bone, **(C)** fluorescent images of the right rear leg bone and major organs from mice euthanized 24 h after i.v. injection, **(D)** kidneys, **(E)** liver, and **(F)** spleen. Data are mean ± S.D. (n = 3, * $p < 0.05$, ** $p < 0.01$).

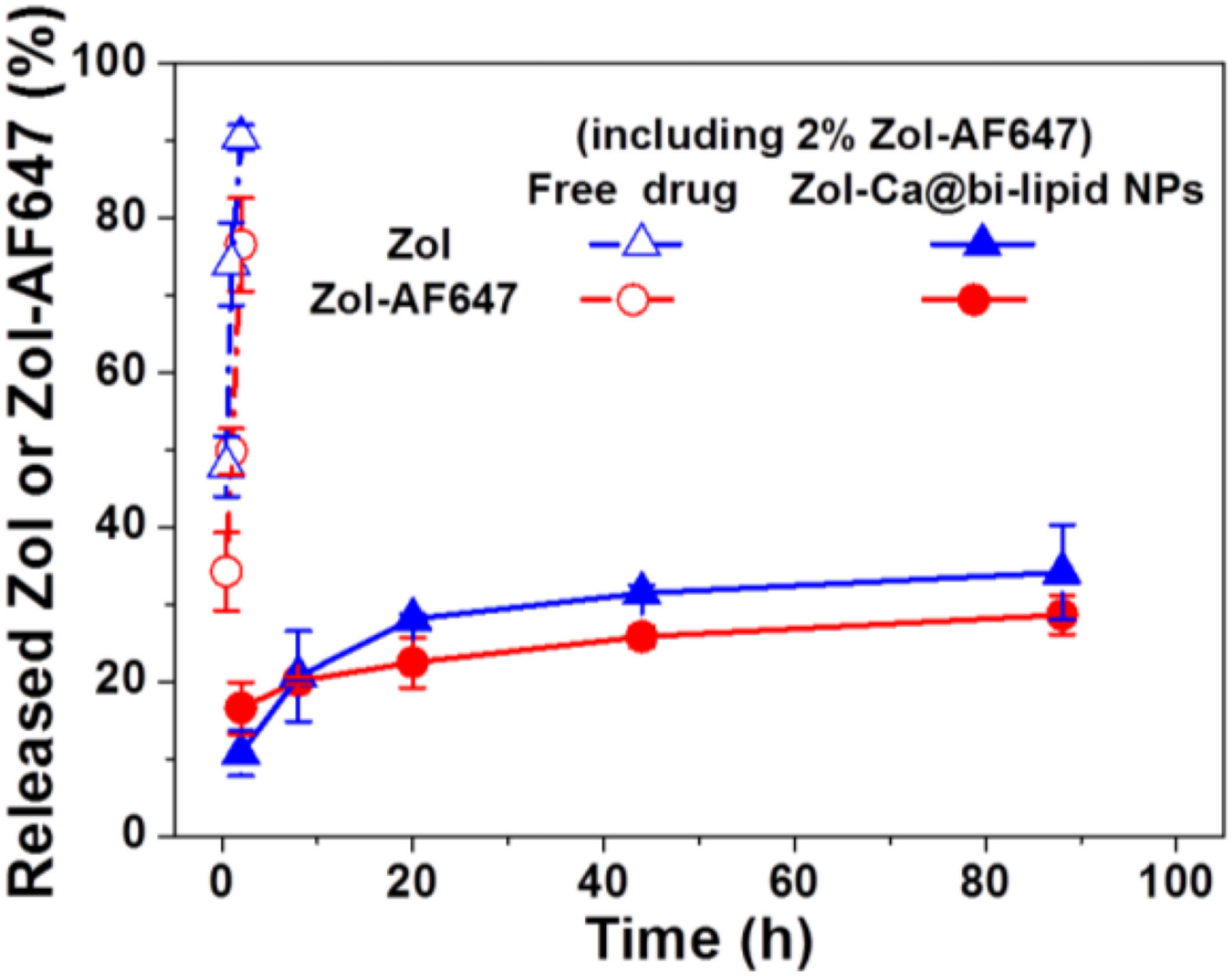

Fig. 6.

A comparison of the release profiles of Zol and Zol-AF647 from the same Zol-Ca@bi-lipid NPs that contain 2% Zol-AF647 in 10 mM sodium phosphate buffers (pH 7.4). Data are mean ± S.D. (n = 3).